Investigation of non-normal incidence charged-particle response of CR39 nuclear track detectors, with applications in nuclear diagnostics for inertial confinement fusion

by

Ryan Przybocki

Submitted to the Department of Physics
in partial fulfillment of the requirements for the degree of

Bachelor of Science in Physics

at the

MASSACHUSETTS INSTITUTE OF TECHNOLOGY

May 2020

Author . . . . . .
Department of Physics

Certified by. . . . . .
Maria Gatu Johnson
Research Scientist, MIT Plasma Science and Fusion Center
Thesis Supervisor

Certified by. . . . . .
Richard Petrasso
Senior Research Scientist, MIT Plasma Science and Fusion Center
Thesis Supervisor

Accepted by . . . . . .
Nergis Mavalvala
Associate Department Head, Department of Physics

Investigation of non-normal incidence charged-particle response of CR39 nuclear track detectors, with applications in nuclear diagnostics for inertial confinement fusion

by

Ryan Przybocki

Submitted to the Department of Physics
On 7 May 2020
in partial fulfillment of the requirements for the degree of
Bachelor of Science in Physics

Abstract

CR39 is a plastic nuclear track detector used at inertial confinement fusion (ICF) facilities to characterize the energy spectra of fusion products. This thesis presents data collected at MIT's Linear Electrostatic Ion Accelerator (LEIA) to measure CR39's detection efficiency for protons at non-normal incidence to CR39 detectors. We specifically study protons resulting from D-D fusion reactions with incident angles up to 50 degrees. Understanding the CR39 response to charged particles at an angle is essential to designing a D-D neutron spectrometer at the Z facility, which uses CR39 to detect protons incident at an angle. We find that small adjustments of 10 degrees have no effect on detection efficiency, and high detection efficiency is preserved up through 25 degrees in the range of 1.0 to 2.1 MeV. For the ICF applications, incident angles above 30 degrees are generally impractical for spectrometer design due to significant drops in proton detection. We compare the experimental results to related theoretical simulations, proposing significant constraints on these theoretical models of detection efficiency.

Thesis Supervisor: Maria Gatu Johnson
Title: Research Scientist, MIT Plasma Science and Fusion Center

Thesis Supervisor: Richard D. Petrasso
Title: Senior Research Scientist, MIT Plasma Science and Fusion Center

Acknowledgements

I extend my deepest gratitude to Dr. Maria Gatu Johnson for her continued guidance and support through the duration of this research project. In addition, I would like to thank Dr. Richard Petrasso for welcoming me into the HEDP group at MIT where I began my journey into the field of fusion.

This project would not have been possible without the support of the entire HEDP group, and particularly graduate students Brandon Lahmann and Graeme Sutcliffe, who have been invaluable resources along every step of the way.

Contents

List of Figures

List of Tables

1. Introduction

Inertial Confinement Fusion

This project investigates questions in charged particle spectrometry for inertial confinement fusion (ICF) experiments. Characterizing the energy spectrum of fusion products is important to our understanding of the reactions themselves and the conditions under which they occur.

In an inertial confinement fusion experiment, millimeter sized capsules are filled with fusion fuel, such as deuterium and tritium, then imploded using high energy lasers [1]. When a capsule is compressed this violently, the density and temperature of the fuel quickly rise to conditions similar to those in the interior of a star. Under these conditions, the fuel will undergo nuclear fusion and release energy and characteristic charged particles. This method of achieving nuclear fusion reactions is known as inertial confinement fusion.

During the implosion, the fusion of the fuel produces high energy alpha particles, protons, and neutrons. In an ICF ignition scheme with high levels of compression, charged particles remain in the fuel, providing heat for reactions to continue, while neutrons fly out of the capsule. In lower compression experiments (non-ignition), charged particles can also escape. By measuring the energy spectrum of these particles, we can diagnose the performance of an implosion, specifically uncovering information about particle yields, fuel temperatures, fuel densities, and implosion symmetry.

A number of reactions occur in ICF experiments, each with unique products and energies. The fusion of two deuterons (hydrogen nuclei consisting of one proton and one neutron, denoted "D") results in two possible reactions that occur with roughly equal probability [2]:

$$D + D \rightarrow T^{*}\ [1.01\ \text{MeV}] + p^{*}\ [3.02\ \text{MeV}]$$

$$D + D \rightarrow n\ [2.45\ \text{MeV}] + {}^{3}He^{*}\ [0.82\ \text{MeV}]$$

In our experiment we will focus specifically on the first of these reactions and detection of the resulting proton (p*).

CR39 track detectors

In this experiment, we will characterize properties of CR39 (chemical composition $C_{12}H_{18}O_7$), a plastic nuclear track detector used at ICF laser facilities such as Omega [3], Z [4], and the NIF [5] [6] [7]. At these facilities, detector insensitivity to background radiation such as X-rays and electromagnetic noise is paramount, so the detection through mechanical means such as CR39 is preferred as it avoids the background problems associated with electromagnetic detectors.

When an energetic charged particle collides with CR39, it damages molecular chains leaving behind a characteristic track. The tracks are revealed through chemical etching with NaOH, which removes material on the surface of the detector as well as inside the tracks. The rate at which tracks are etched ("track etch rate") is faster than the rate at which the rest of the plastic is etched ("bulk etch rate"), so the tracks are visible after etching as more track material is removed than surrounding material. These tracks in the plastic vary in diameter and depth, in relation to the rate at which the incident particles lose energy, dE/dx. The tracks are then viewed through a microscope that scans the CR39 and tabulates parameters such as track diameter and density. The tracks generally appear circular and symmetric for particle trajectories normal to the CR39's surface. An example is shown in Figure 1. Analysis of the track diameters then enables a measure of the incident energy of particles leaving the tracks. Procedures for relating the response of CR39 to the properties of normally incident protons is well described by Seguin [2003] and Sinenian [2011] [7] [8].

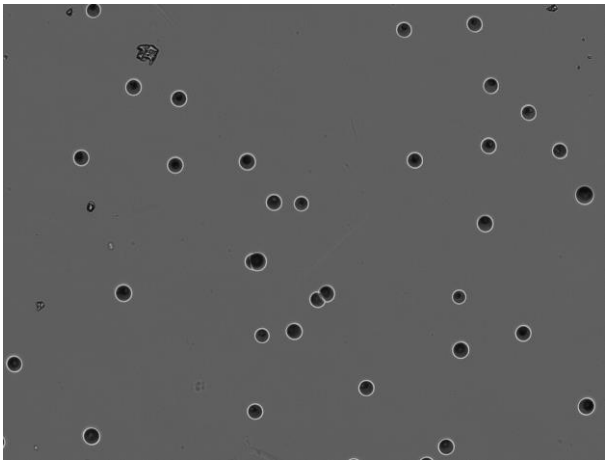

Figure 1: Sample microscope scan image of CR39. Black circles each represent one proton track.

We will refer often to the "detection efficiency" of CR39 under different conditions. This is defined as the ratio of the number of incident particles experimentally detected by the CR39 to the number expected. Seguin [2003] gives a CR39 proton detection efficiency of 100% for incident energies between about 0.5 MeV and 6 MeV.

However, these observations for detection efficiency assume protons at normal incidence to the CR39. The response to protons incident at an angle is less certain. Moreover, certain simplifications to the analysis of normally incident particles are not possible when the particles are incident at an angle, such as automatically filtering out non-circular tracks that usually only appear as background noise. Understanding CR39 response under angled incidence is important for neutron spectrometer designs that involve detecting recoil protons at an angle. Figure 2 illustrates a detector design using that concept [9]. The purpose of this project is to characterize the detection efficiency of CR39 for protons incident at an angle. We specifically choose to study protons resulting from the fusion of two deuterons, which have a known average energy of 3.02 MeV.

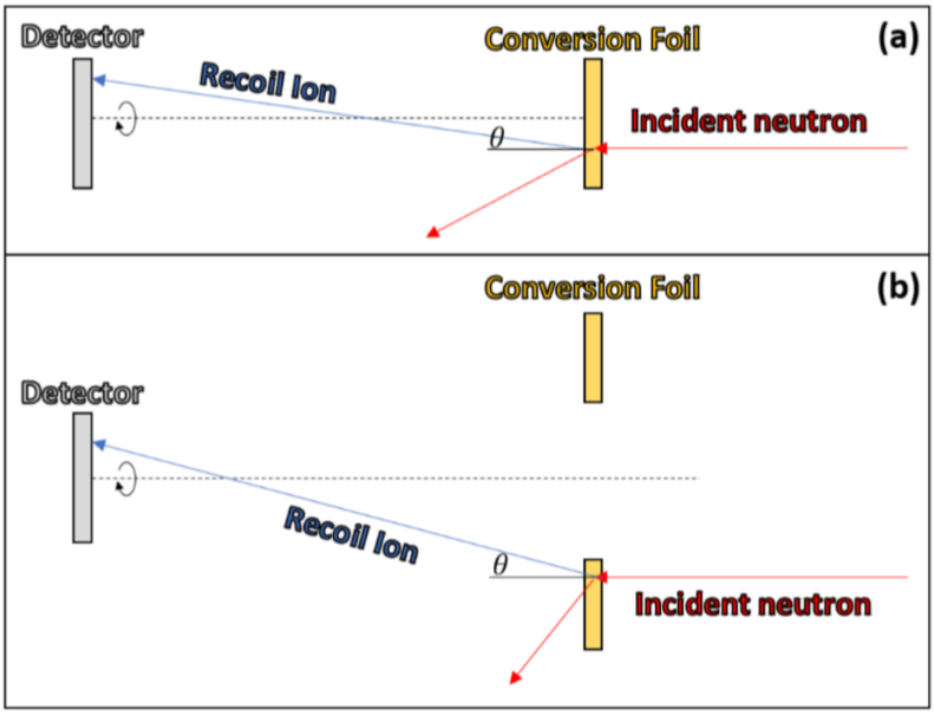

Figure 2: Neutron spectrometer concepts proposed by B. Lahmann et al. for detection of D-D neutrons [9]. Incident neutrons pass through a conversion foil, colliding elastically with ions. These recoil ions are scattered at an angle, some of which reach a CR39 detector at a non-normal incident angle.

Facility

The fusion experiments in this paper were carried out in MIT's Linear Electrostatic Ion Accelerator (LEIA), a facility that develops diagnostics for Omega, Z, and the NIF [10]. In our experiments, a high voltage (125 kV) accelerates deuterium ions down the beam line and onto an Erbium-Deuteride (ErD_2) target in order to produce D-D fusion products. User ports extending off the target chamber allow us to place CR39 detectors for our experiments. An overview photo of LEIA is shown in Figure 3.

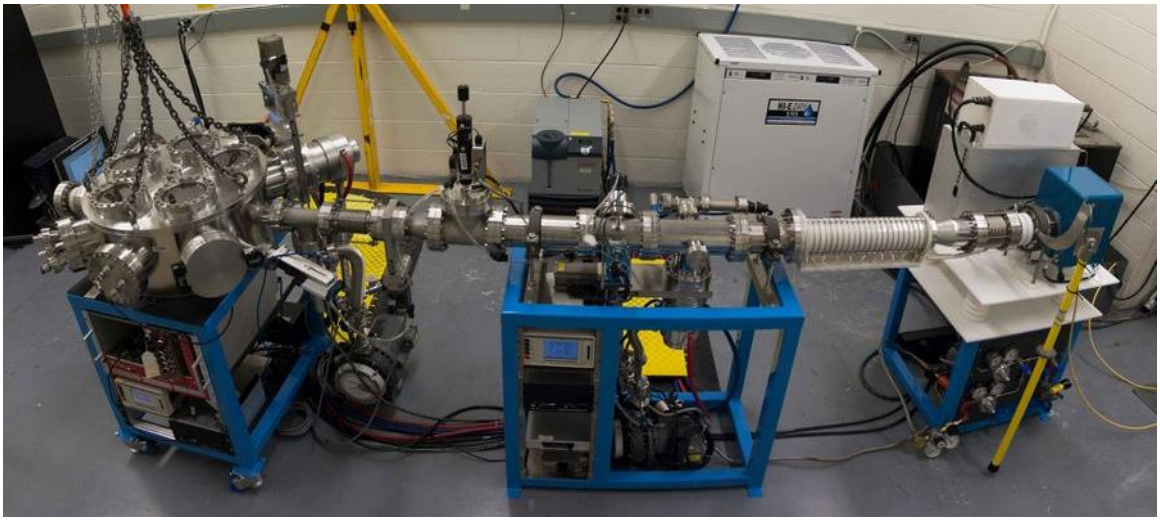

Figure 3: MIT's Linear Electrostatic Ion Accelerator (LEIA). From left to right: cylindrical target chamber, beam line, ion source (in blue shielding). Photo from Sinenian et al (2012) [10].

2. Experiment Design

We design an experiment at the accelerator facility that investigates the detection efficiency response of CR39 to protons with angled trajectories. Comparisons are made between the detection efficiency and variables of incident angle, incident energy, and CR39 etch time.

Energy Selection Filters

The D-D fusion reaction of interest yields a proton with an energy of 3.02 MeV. We can study energy values at or below this value by introducing range filters that reduce the kinetic energy of these protons. In normal incidence experiments, filters are commonly used in front of CR39 in applications that involve incident energies above 6 MeV to scale down to the regime of 100% detection efficiency [7].

A commonly available material to use as a filter is aluminum, which comes in a variety of thicknesses. Using a program for the Stopping and Range of Ions in Matter (SRIM) developed by Ziegler [11], we can compute the transmitted energy of protons with a known incident energy on an aluminum filter, as a function of aluminum thickness.

We choose a simple range filter (SRF) design, which implements fixed filter thicknesses to yield discrete incident energies on CR39. To limit the number of independent trials we need, we design a filter arrangement to include 6 individual filters overtop one 5 cm CR39 round. A schematic for the filter design is shown in Figure 4, where the individual sections are numbered 1 through 6 in order of increasing thickness.

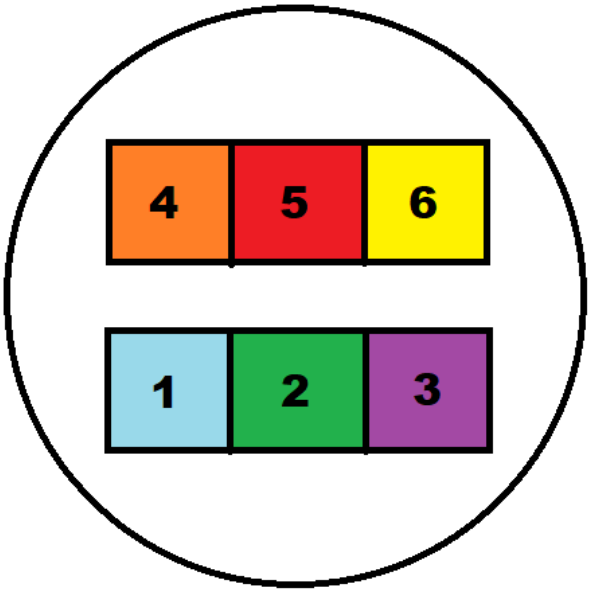

Figure 4: Schematic for filter arrangement that includes 6 different aluminum thicknesses.

Our goal was to design these filters to obtain 6 energy values spaced between approximately 0.5 MeV and 3.0 MeV. For ease of construction, filters 1 and 4 consisted of one base layer of aluminum each, while filters 2, 3, 5, and 6 were constructed by adding successive layers on top of the existing base layers. Note that we did not space the energy values perfectly equally due to constraints on the thicknesses of aluminum available. The nominal layer thicknesses and predicted energies are shown in Table 1.

Table 1: Nominal filter thicknesses and their energies predicted by the SRIM calculator

Filter	Al thickness (μm)	Predicted energy (MeV)
1	6	2.88
2	24	2.44
3	39	2.03
4	50	1.68
5	62.5	1.21
6	75	0.58

Filter Calibration

The first set of experiments were done to measure the six filter energies and calibrate their true thicknesses. The predicted energy values in Table 1 assume that the quoted aluminum thicknesses are exact, when in reality there is some uncertainty associated with manufacturing the aluminum. Experimentally determining the energy will give us more accurate values for filter thicknesses. These are referred to as the "filter calibration runs."

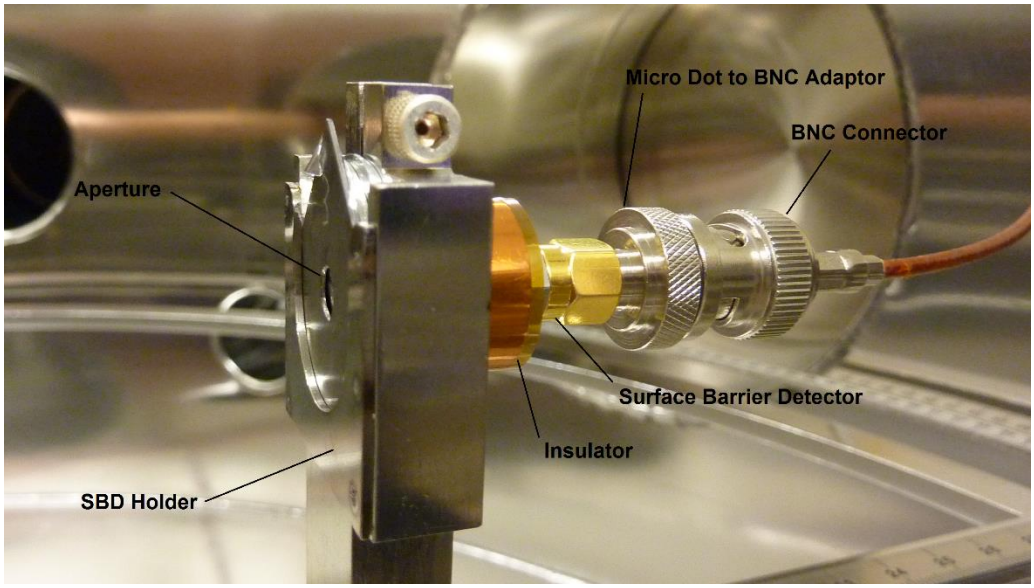

Figure 5: Close-up view of an SBD inside the target chamber of LEIA, showing the aperture, detector, and output. A second SBD (not shown) is situated in the chamber but is unused for this part of the experiment. Picture from LEIA wiki [12].

To experimentally determine the energies of protons passing through our filters, we use Silicon Surface Barrier Detectors (SBD's) positioned in the target chamber of LEIA, as shown in Figure 5. The SBD is a semiconductor device in which charged particles produce electron-hole pairs that send a pulse which is then amplified and processed by a multi-channel analyzer [12]. The SBD's are energy calibrated using an alpha source with five known energies (^{226}Ra).

For these calibration runs, we use data from an SBD positioned 22.724 cm away from the target. An aperture with area 0.086 cm^2 is placed in front of the detector to restrict the area of the

detector for more accurate energy measurements. We place the filter section of interest directly in front of the aperture. This arrangement is shown in Figure 6.

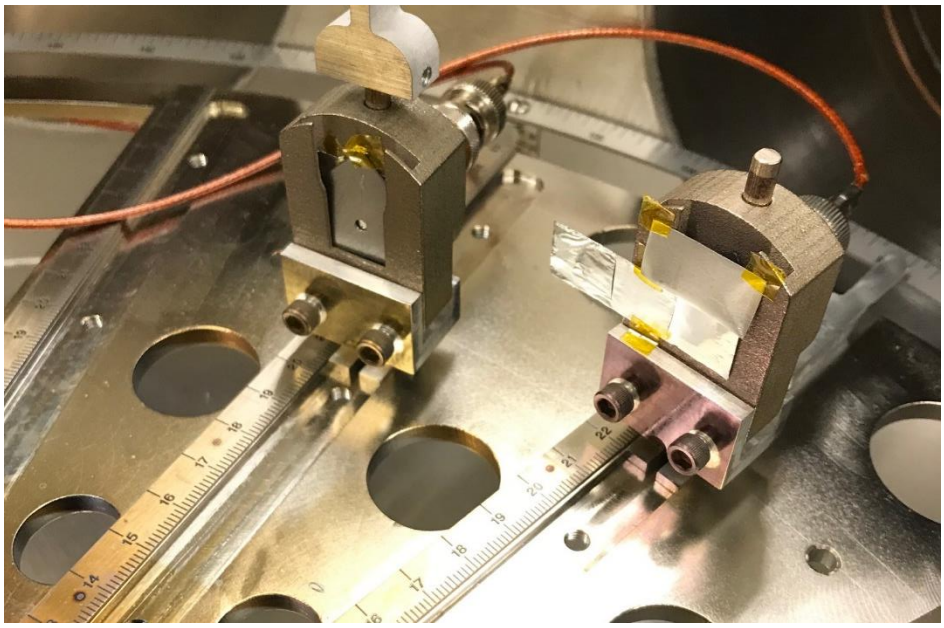

Figure 6: Setup for filter calibration runs, showing part of the filter arrangement over the SBD aperture (right).

Trials were done with this setup on all 6 filters. We aimed for approximately 3500 proton counts on the SBD to provide sufficient statistics in our data for an accurate mean energy fit. The proton counts are binned according to their incident energy by the CAEN Multi-channel Analyzer (MCA), to a resolution of 0.544 keV. A sample histogram of energies is shown in Figure 7.

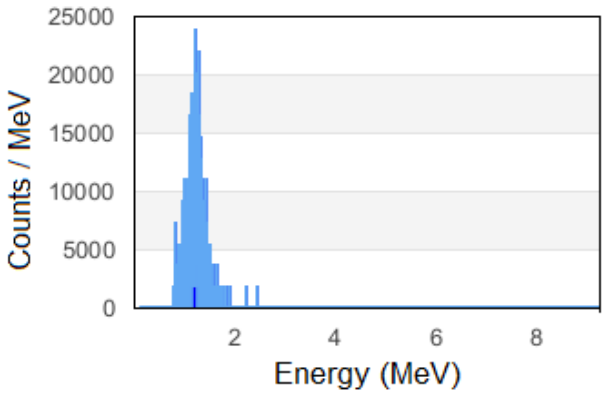

Figure 7: Sample histogram from multi-channel analyzer for a filter calibration run.

The analysis of the MCA data in the filter calibration runs is straightforward. The MCA outputs comma separated values of incident energy and number of counts at that energy. By plotting these values and averaging over energy we obtain the mean energies of D-D protons passing through the aluminum filters. The values (in MeV) obtained through this procedure are shown in Table 2.

Table 2: Measured energy values of protons passing through filters and actual thickness as determined by SRIM

Filter	Measured Energy (MeV)	Actual thickness (μm)
1	2.898	5.36
2	2.471	22.87
3	2.063	37.72
4	1.668	50.29
5	1.201	62.75
6	0.740	72.35

In the remainder of the experiment, we use these measured values as the baseline energies for protons passing through the filters at normal incidence. The SRIM calculator can then determine the actual thicknesses of the six filters from their energies. These values offer a correction to the nominal thicknesses listed in Table 1, and we use this actual thickness going forward.

Given that we are studying the behavior of protons incident at an angle, we must consider the change in incident energies arising from filters positioned at an angle. An angled offset θ

effectively increases the thickness of the filter by a factor of 1/cos(θ) (we take θ as the angle of offset away from normal incidence).

Due to the positioning of the SBD, it is difficult to carry out these filter calibration runs at non-normal incident angles, and doing so would require a large number of calibration runs. Thus we do not directly probe the filter energies when they are positioned at an angle. However, we can make calculations based on the SRIM data. In each trial, there is a known angle offset θ. Using θ and the actual aluminum filter thickness we can then compute the thickness of the angled filter. Finally, we use this angled filter thickness in the SRIM calculator to compute the energy of protons passing through the filters at angled incidence.

Preliminary Setup Considerations

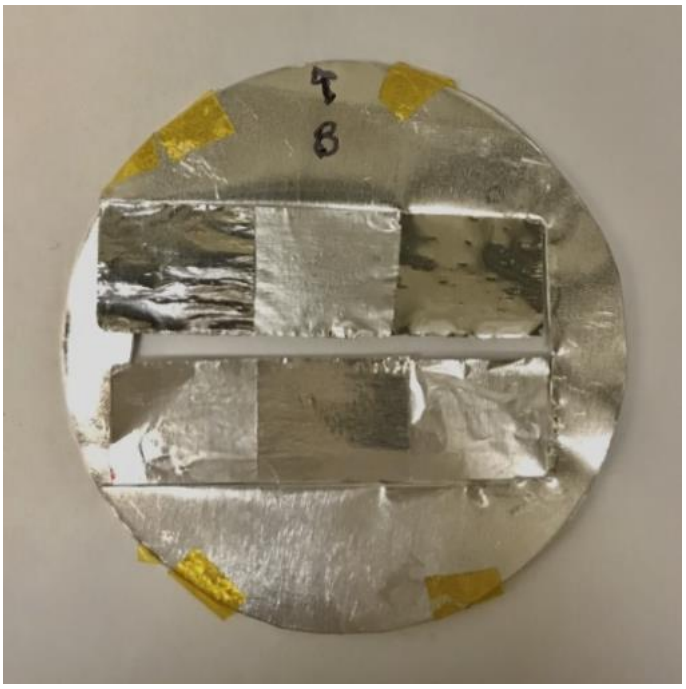

Figure 8: Filter setup designed to fit over a 5 cm CR39 round.

The aluminum filter setup (Figure 8) is encased between two thicker aluminum circles and designed to fit over a 5 cm CR39 round. This arrangement is held in place by custom machined

parts that maintain the filter positioning. The casing is then mounted on a rotating pedestal that measures the angle offset with respect to the base of the mounting hardware. The casing, pedestal, and angle gauge are shown in Figure 9. This setup is placed inside the extension to the accelerator chamber during operation of the experiment, at the position shown in Figure 10. By measuring the precise position of this pedestal with a depth gauge, we determined that there was a constant +0.35º offset that must be added to the reading on the angle gauge.

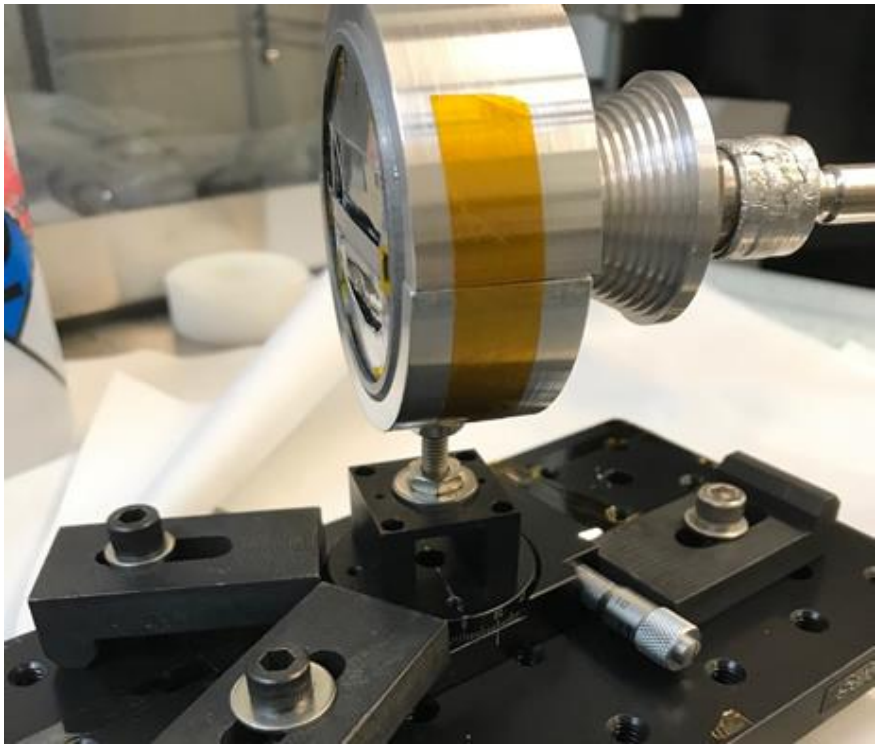

Figure 9: Casing for CR39 and filters, mounted on a rotating pedestal with an angle readout.

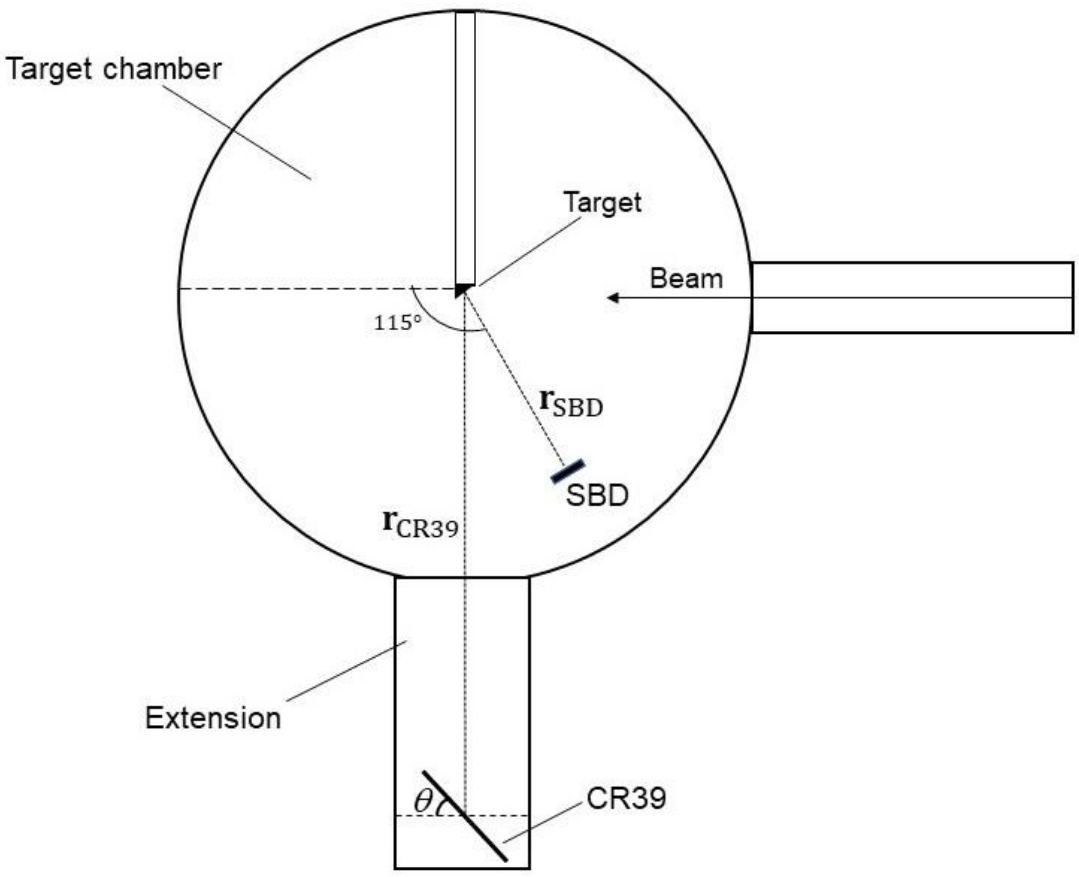

Figure 10: Top view of the target chamber and extension, showing the direction of the incident beam, the ErD_2 target, the position of the SBD, and the CR39 offset at an angle θ. Not drawn to scale.

Due to the customized setup of the CR39, our measurements of various distances must be made by hand. The positions of the CR39 setup and the SBD detector relative to the target are shown in Figure 10.

The flux of charged particles reaching the CR39 depends on the inverse square of the distance r_{CR39} from the target, so an accurate measurement of this distance is important for analyzing CR39 flux. In a series of measurements with the CR39 setup in place, we found the horizontal distance to average 62.8 ± 0.5 cm, while the vertical offset was 3.05 cm for the lower row of filters (1, 2, 3), and 4.55 cm for the upper row (4, 5, 6), making the distances from the target to the lower and upper rows 62.87 ± 0.5 cm and 62.96 ± 0.5 cm, respectively.

We also require the SBD maintain a known position relative to the target across experimental trials. The primary SBD in our experiment is positioned with its base at the 17.0 cm demarcation in the accelerator. These distance markers were found to be accurate to within approximately 2 mm. The SBD aperture is known to be 0.724 cm behind the base, so the target to aperture distance r_{SBD} is measured to be 17.724 ± 0.2 cm. It should be noted that the SBD aperture for this experiment is different than that used for the filter calibrations. The new aperture has an area of 0.172 cm^2.

The experiment aims for approximately 20 proton tracks in CR39 per microscope frame to reflect expected conditions in the proposed neutron spectrometers. This corresponds to roughly 16700 tracks per cm^2 in CR39 given a frame area of 0.12 mm^2. We then estimate the number of SBD proton counts needed to get 16700 tracks/cm^2 on the CR39, using the known aperture area of the SBD and the fact that the particle fluence falls off with the square of distance.

With this flux relationship, we find that we need approximately 37000 counts on the SBD to achieve 20 tracks per frame in CR39. Further corrections to this approximation will be introduced when we analyze our CR39 data to account for the angle between the CR39 and SBD.

3. Experiment

Procedure

A consistent experimental procedure is followed for all the main trials on angled CR39, while only varying the angle offset of the CR39. The filters are aligned the same way each time, with the rows (1–3) and (4–6) parallel to the base of the holding apparatus, and the CR39 round held in place directly behind the filters. The platform holding the CR39 is placed on tracks within the accelerator's extension that enables a consistent setup at the same distance. The angle of the CR39 is set before placing the platform inside the accelerator and checked again once inside and in place. We did trials with the following angles (in degrees): 0, 10, 20, 25, 30, 35, 40, 45, 50.

An overview of the setup in the accelerator chamber is shown in Figure 10. With the apparatus in place, we then check the positioning of the SBD to ensure consistency across trials. Once all necessary adjustments are made, the accelerator is closed and standard LEIA operational procedures are followed for vacuum pumping and high voltage [13]. As before, we operate the accelerator with a deuterium ion beam to produce 3.02 MeV protons as the fusion product of interest.

Once the plasma beam is extracted and counts begin to appear on the MCA, we continue until we reach approximately 37000 counts, at which point we stop plasma extraction and follow consistent procedures to open the accelerator chamber and collect the CR39.

Data Processing

The CR39 is processed first by etching with NaOH then scanning with a microscope that tabulates the proton tracks through the ScanCR39 program. Each piece of CR39 is first etched for 2 hours with additional etching of 2 hours and 1 hour following this, such that each accelerator trial has scanned data from 2, 4 and 5 hour etch times.

The scan data is imported into the 'AnalyzeCR39' program devised by F. Seguin. This program allows one to isolate sections of a scanned CR39 piece and perform various functions to find average proton track density, contrast, diameter, and eccentricity. Track density (tracks/cm^2) is what we use to compare the flux of protons in CR39 to that in the SBD. Contrast is defined in this case as (100% - optical contrast in %), i.e. the darkest proton tracks have the lowest contrast and vice versa. Eccentricity is a measure of the roundness of the tracks, with a higher value denoting a more oblique track.

CR39 Track Yield

We devise a method to compare the proton tracks/cm^2 across different CR39 arrangements. To normalize these to a common baseline, we use our observed CR39 flux (in tracks/cm^2) and divide by the theoretical expected flux, which comes from the SBD flux, adjusted for the different distance and orientation with respect to the target of the SBD versus the CR39. This number is the percent detection in CR39 relative to the SBD, which we use as the detection efficiency.

The theoretical expected flux is related to the SBD flux by the inverse square law. We also consider that the angle offset of CR39 reduces its cross-sectional area available for incident protons by a factor of cos(θ). Finally, we include a correction factor to account for the different angular positions of the SBD detector and the CR39. In data from accelerator facility characterization collected outside the scope of this work, the yield for an SBD at an angle of 115 degrees (relative to the beam line) is 0.9676 times that of an SBD at 90 degrees (the position of the CR39) [10]. Combining these contributions, we obtain the following relationship between expected CR39 flux (tracks/cm^2) and observed SBD counts:

$$\Phi_{\mathrm{CR39,\,expected}} = \frac{C_{\mathrm{SBD}}}{A_{\mathrm{SBD}}} \cdot \left(\frac{r_{\mathrm{SBD}}}{r_{\mathrm{CR39}}}\right)^2 \cdot \cos(\theta) \cdot \frac{1}{0.9676}$$

Where C_{SBD} is the number of counts observed on the SBD, and A_{SBD} is the SBD aperture area (0.172 cm^2 in our experiment).

The main contribution to error in our expected flux comes from the uncertainty in the two distance measurements, r_{SBD} and r_{CR39}. From our earlier measurements, where we estimated r_{SBD} to be correct to ±2 mm and r_{CR39} to ±5 mm, we estimate the error on this flux measurement to be 4%. This provides us with a lower bound for error bars when comparing measured flux to expected flux for detection efficiency.

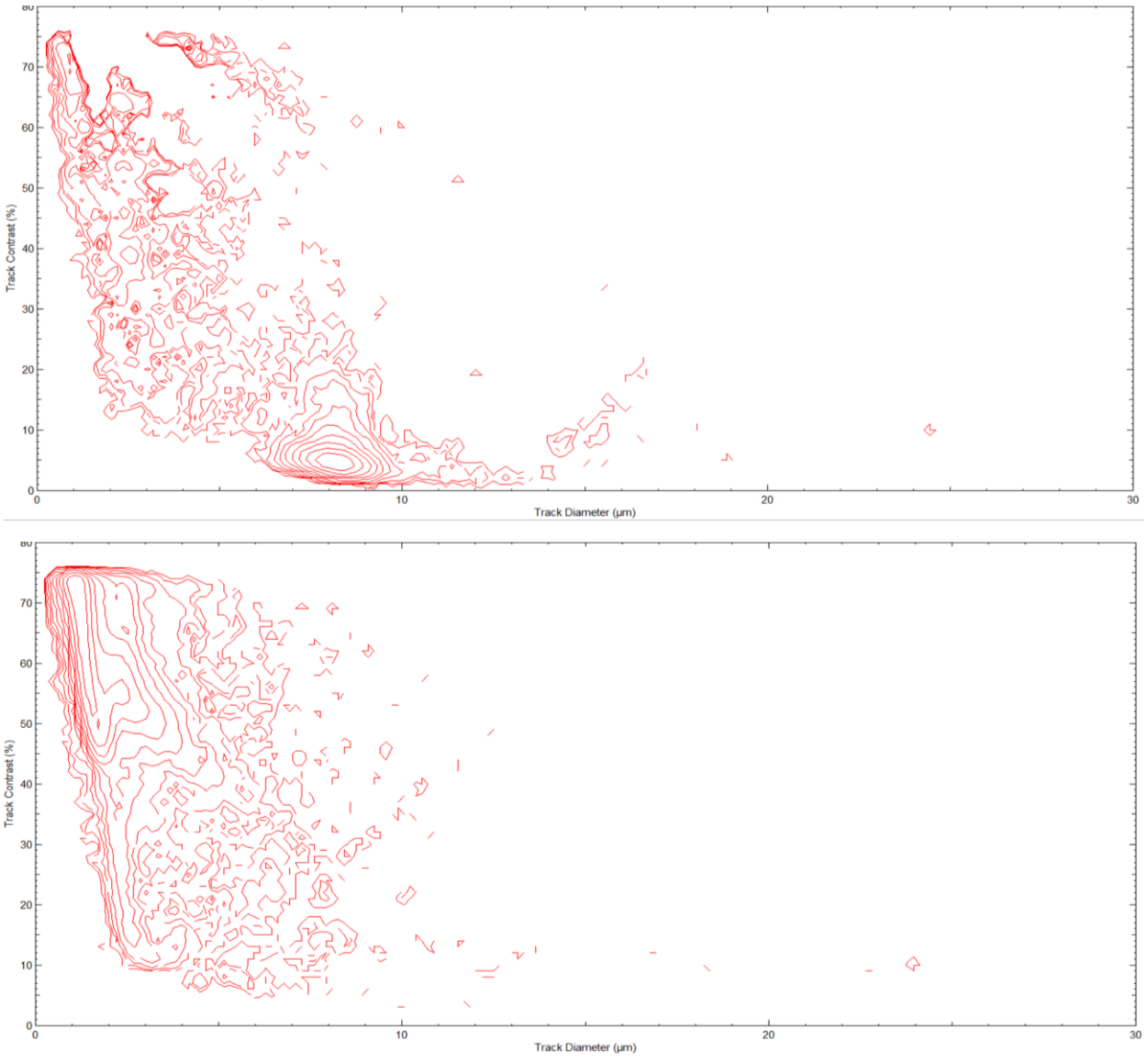

Figure 11: Example contour plots of track contrast vs diameter for a section of CR39, in the 'AnalyzeCR39' analysis software. Note the well-defined contour peak at about 8 µm on the top plot. This represents the signal, which is easily separable from the higher contrast background noise. Compare with the bottom plot, where the signal begins to blend with noise at higher contrasts.

For CR39 arrangements that yield a significant number of high contrast (lighter colored) tracks, additional sources of error must be considered, specifically the high number of background tracks that obfuscate the data. Typically, for reasonably low contrast groupings, the proton signal tracks are concentrated and distinct from high contrast background noise. However, in cases where the proton tracks cannot be isolated from the background noise on the CR39, resolving the precise number of tracks is not possible. Examples of both cases are shown in Figure 11. We introduce an additional source of error for the case where signal cannot be properly separated from noise, based on the scans of background noise by B. Lahmann (see Figure 12).

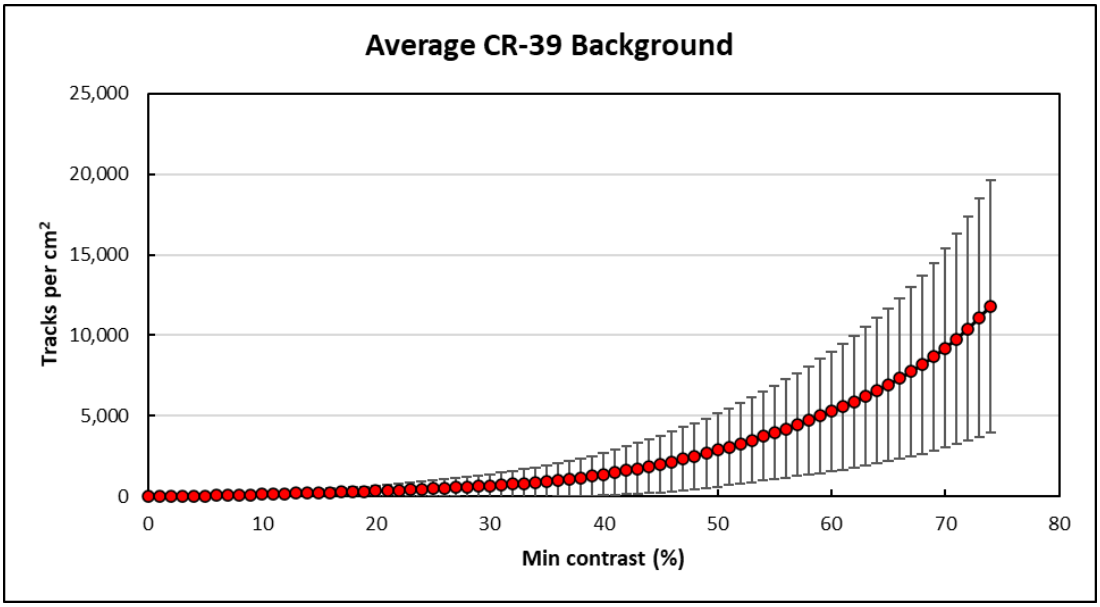

Figure 12: Average level of background noise at contrast levels up to 75%.

We derive an uncertainty figure based on the observed error for the number of background tracks, shown in Figure 12. In doing our analysis, we perform a background subtraction for the CR39 piece then use the remaining data to find track yield. The fractional uncertainty on this resulting data scales linearly with the background uncertainty, and inversely with the measured number of proton tracks, making the overall fractional error contribution equal to $\beta/\Phi_{\text{measured}}$, where β is the value of background noise.

Summing this background noise uncertainty with the distance measurement uncertainty of 4% in quadrature, we obtain a relative uncertainty on the measured flux in CR39:

$$\frac{\sigma}{n} = \sqrt{0.04^2 + \left(\frac{\beta}{\Phi_{\text{measured}}}\right)^2}$$

4. Results

The analysis of our data can be sorted according to a number of variables that affect the proton detection efficiency of CR39, namely angle of incidence, proton energy, and CR39 etch time.

From an initial overview of the data, we first notice the difficulties of detection at large angles. The scan of CR39 placed at 50 degrees yields data that is indistinguishable from noise at all etch times, so we establish a general upper range of detection to be 45 degrees. At 45 degrees, detection is still extremely limited, and the only detection efficiency that is not within error of zero comes from filter 4 at 1.1 MeV. We thus consider these highest offsets of $\geq 45^{\circ}$ to be entirely impractical for spectrometer design.

Angle dependence at a fixed energy

A confounding variable in our analysis is the proton energy after passing through the filter. As discussed previously, the effective aluminum filter thickness increases as the angle offset of CR39 increases, introducing a dependence on angle for the filter energy. We expect the proton energy to have an effect on the detection by CR39, so ideally we could keep energy fixed to compare across different angles. This limitation of effective filter thickness (and thus incident energy) changing makes the task of comparing detection efficiencies more difficult.

We start by noting that for the thinnest, higher energy aluminum filters, the incident energy changes very little as the angle is increased. Specifically, at 40 degrees filter 1 yields an estimated incident energy of 2.86 MeV, nearly identical to the energy of 2.898 MeV at 0 degrees. We can thus, to a good accuracy, approximate filter 1 as a constant 2.9 MeV filter.

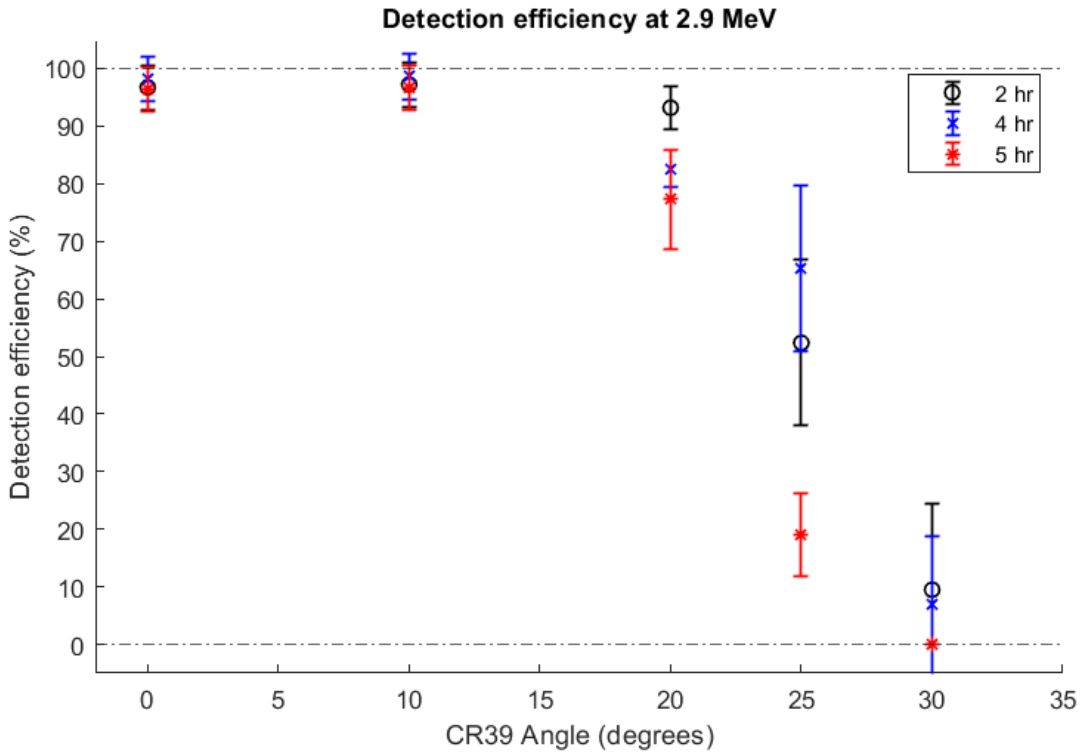

Figure 13: Detection efficiency for filter 1 (2.9 MeV) at angles up to 30 degrees. Plot includes data for all three etch times (2, 4, and 5 hours).

The results of this analysis with filter 1 are shown in Figure 13. We stop our plotting at 30 degrees beyond which the detection efficiency is within error of zero. As seen in the figure, the detection efficiency at 0 degrees is within error of 100% as expected. The data is virtually unaffected by the 10 degree offset, remaining within error of 100%. Additionally, at 0 and 10 degrees, little to no difference is observed between different etch times (2, 4, and 5 hours).

At 20 degrees, we start to see the CR39 detection efficiency decreasing. Only the 2 hour etch retains over 90% of expected tracks. The detection efficiency then falls precipitously, reaching zero within error by 30 degrees. We see that an increase in etch time generally results in the same or worse detection at angles of 20, 25, and 30 degrees.

A similar analysis can be done for filter 2, the second highest energy filter. At 0 degrees, this filter yields an incident energy of 2.47 MeV, which decreases to 2.38 MeV at 30 degrees. We make an approximation of constant energy for this filter, which is reasonable as the energy remains

within 0.1 MeV of 2.4 MeV. Though less accurate than the constant energy assumption for filter 1, this approximation allows us to make a useful comparison to filter 1 in the detection drop off.

The plot for filter 2 is shown in Figure 14. This illuminates a similar pattern to filter 1, with the difference being most of the detection drop off occurs between 25 and 30 degrees rather than 20 and 30 degrees. An increase in etch time appears to have a small but noticeable effect that decreases the detection, as seen in the 20 and 25 degree cases.

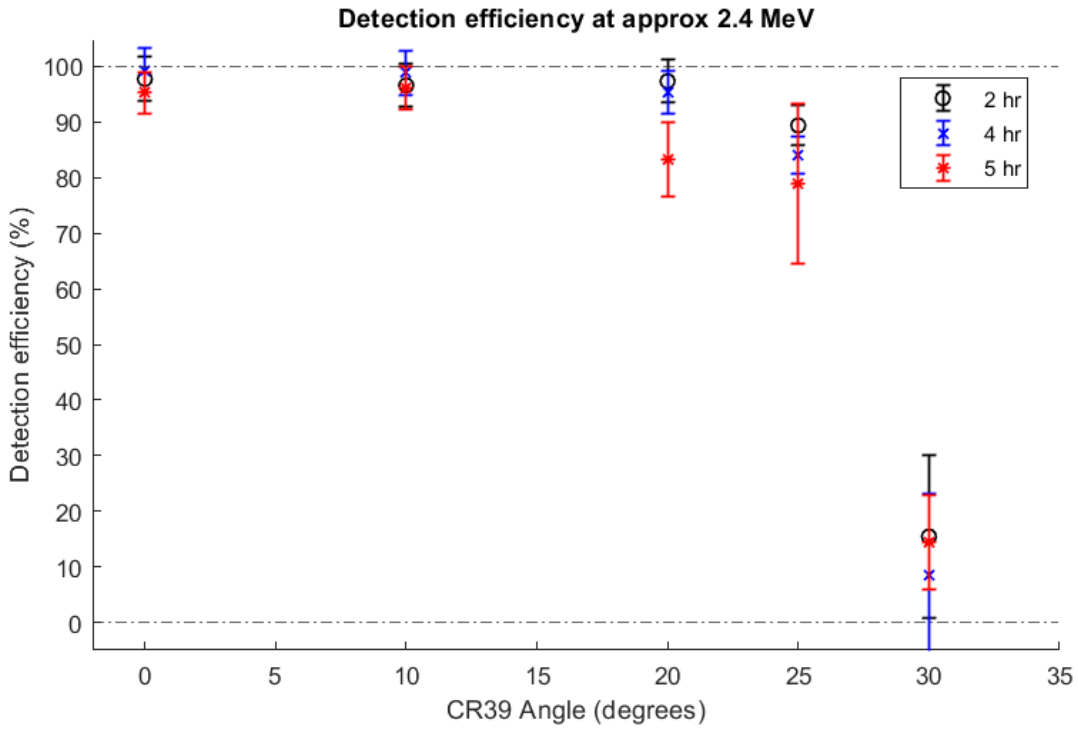

Figure 14: Detection efficiency for filter 2 (~2.4 MeV) for angles up to 30 degrees.

The data from filters 1 and 2 suggests that, if the pattern holds, the "critical angle" (at which proton detection begins to drop significantly) appears to increase as incident energy decreases. That is, the lower energy filters are presumed to maintain higher (>90%) detection efficiency at higher angles. We can also extrapolate to energies above 2.9 MeV and predict that the detection efficiency will begin to drop off at smaller angles as the energy increases.

The limitations on filter design makes it impossible to continue the analysis as before to test this pattern - given that the thicker filter energies vary more drastically with angle, so we can no longer make the constant energy assumption beyond filters 1 and 2. However, we can plot the data as detection efficiency vs. energy for the different angle values in order to probe the response at energies below 2.4 MeV.

The results of this analysis at all etch times are shown in Figure 15. We can see that the energy values begin to spread out and are no longer tightly clustered as they are at 2.4 and 2.9 MeV. As expected, the decrease in energy below 2.4 MeV slightly improved the detection at 25 degrees compared to the 2.4 and 2.9 MeV filters.

At angles up to 25 degrees, the detection efficiencies from approximately 0.8 to 2.1 MeV are within error of one another at 2 hours of etching. Thus, angles less than or equal to 25 degrees have little effect on the detection of protons in this energy range. At 30 degrees, all detection efficiencies are under 90% and not within error of the 0 degree detection.

For the longer etch times (4 and 5 hour), efficiency falls off noticeably faster at low energies (below 1.0 MeV). At these etch times, detection efficiencies from approximately 1.0 to 2.1 MeV are within error of one another up to 25 degrees. Detection efficiency is noticeably reduced at 30 degrees for all energies in this range.

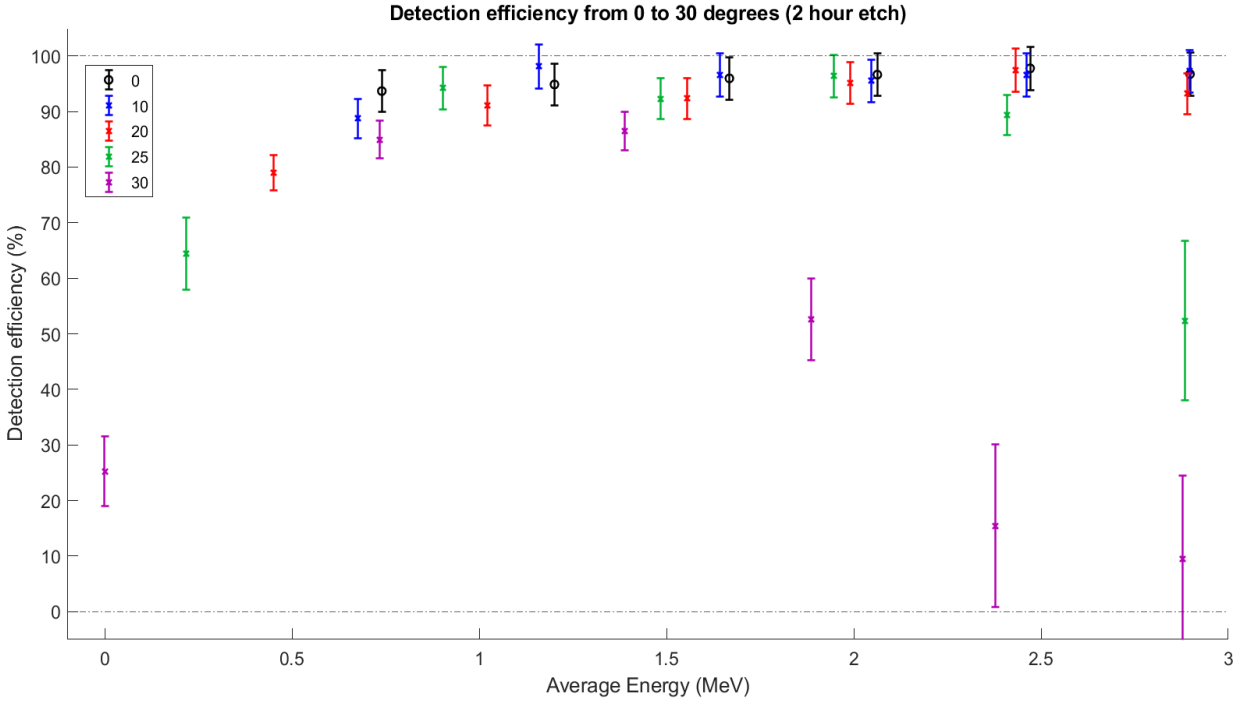
Detection efficiency from 0 to 30 degrees (2 hour etch)
Detection efficiency (%)
Average Energy (MeV)
0
10
20
25
30

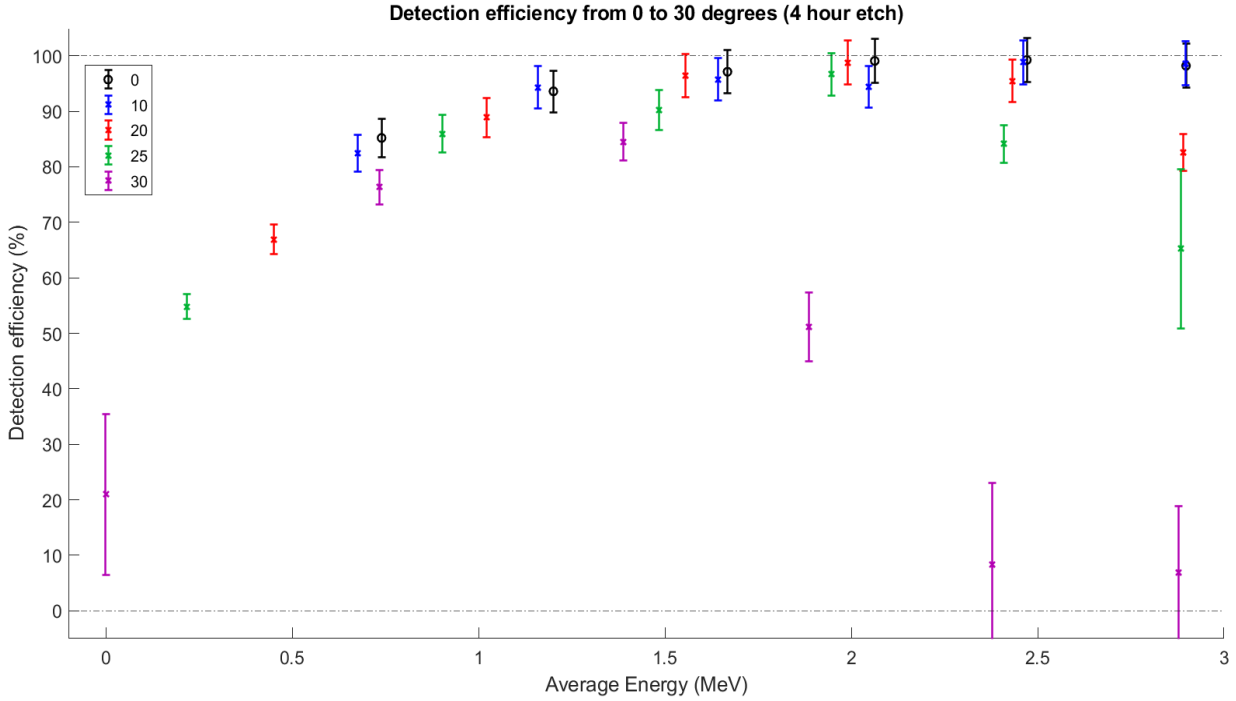
Detection efficiency from 0 to 30 degrees (4 hour etch)
Detection efficiency (%)
Average Energy (MeV)
0
10
20
25
30

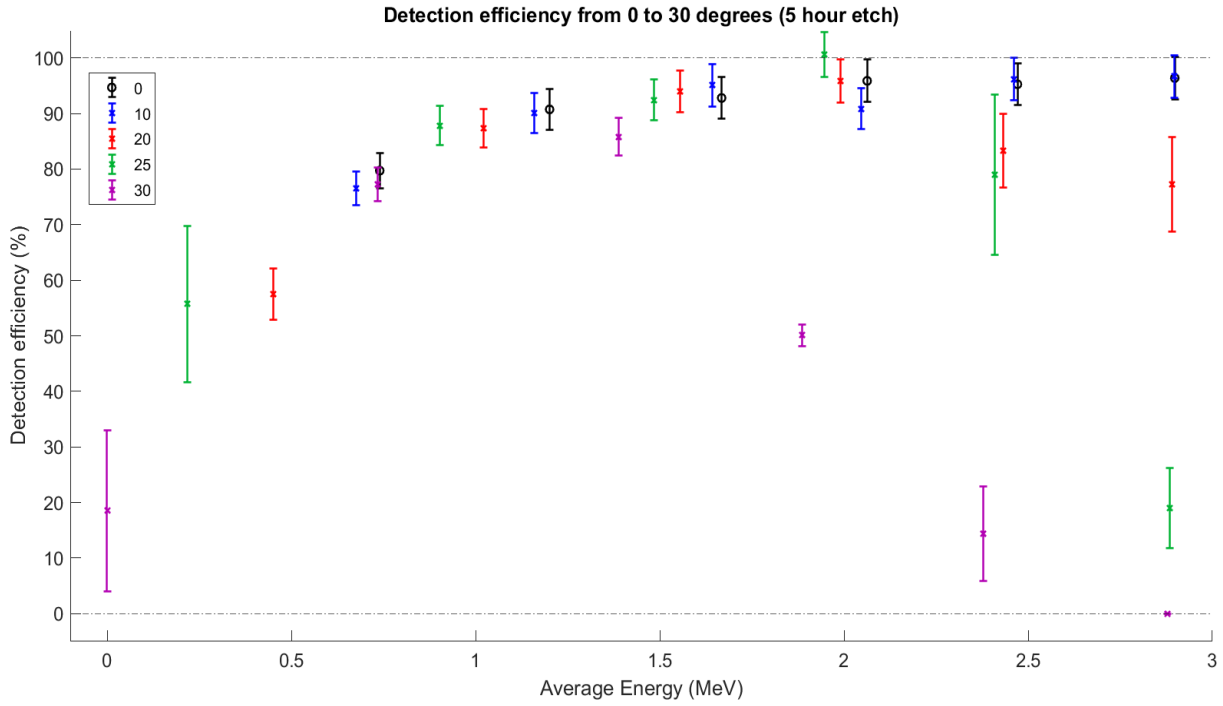

Figure 15: Results of all 2-hour, 4-hour, and 5-hour etch data for angles up to 30 degrees

At low energies, below about 0.8 MeV, the detection efficiency does not hold reliably as it did for the range up to 2.1 MeV. At higher angles, the incident energy decreases and approaches zero. CR39 is estimated to detect 100% of protons normally incident between 0.5 and 6 MeV. Thus it is difficult to pinpoint the cause of the detection drop below 0.8 MeV, which may be attributable to both the angled offset in the experiment and the low energy limitations of CR39. However, at the 4 and 5 hour etch times, we also see the 0 degree, 0.74 MeV proton detection drop below the higher energy protons, so we can conclude that CR39's limitations at low energy are playing at least a partial role in the detection drop off below 0.8 MeV. More trials in this low energy range (0.1 - 0.8 MeV) would be needed to determine the exact behavior of CR39 with low incident energies.

Comparison to theoretical models

These observations offer some constraints on theoretical simulations for detection at high angles. Frenje et al [2003] performed Monte Carlo simulations of normally incident neutrons on CR39 that scatter protons at a spectrum of angles; these simulations modeled detection of protons as a function of the scattering angle [14]. These results are shown in Figure 16.

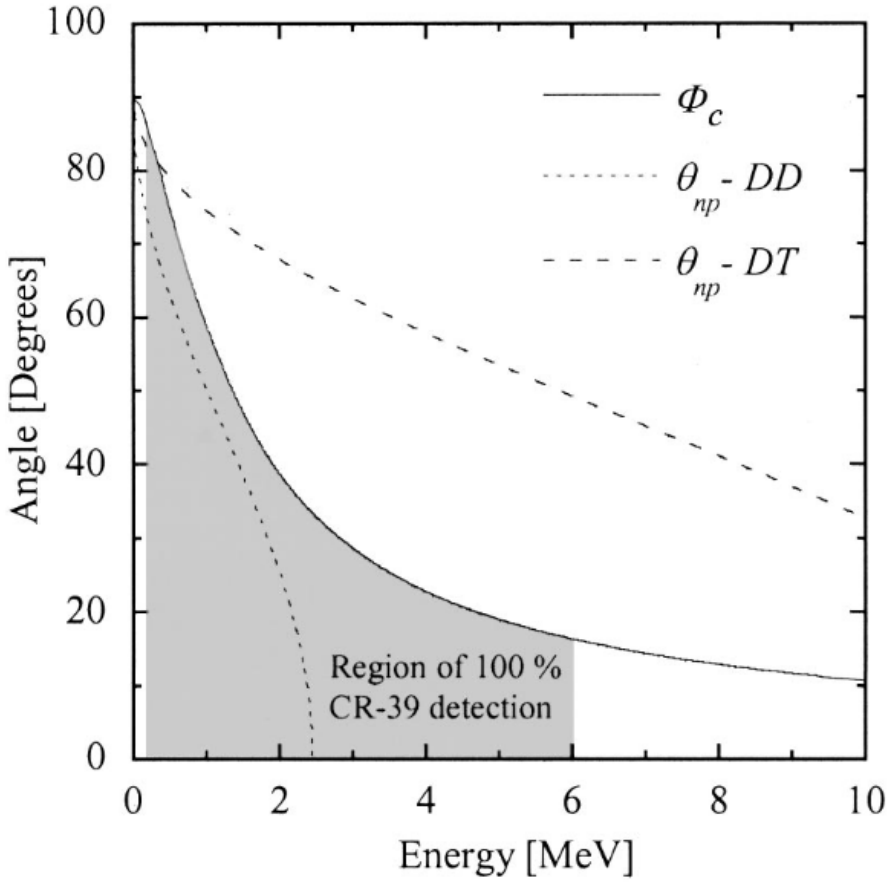

Figure 16: Simulation of CR39 detection of protons scattered at an angle by incident neutrons. The grey region represents a theoretical regime in which the CR39 has 100% detection efficiency. Plot from [14].

In the energy range we are studying (≤ 3 MeV), the model suggests 100% detection efficiency below about 30 degrees. Our experiment found that, at 30 degrees, detection efficiency drops for all filters, and is at or near zero above 2.4 MeV. The model also predicts 100% detection at 45 degrees for all energies below about 2 MeV. The trial run at 45 degrees generated visible

tracks only for one filter, at 1.1 MeV, and beyond 45 degrees our data was indistinguishable from noise. Our experiment determined that this model of scattered protons does not hold for our experiments involving protons incident at an angle.

5. Summary

This experiment has focused on the CR39 detection of protons resulting from the D-D fusion reaction that yields protons at 3.02 MeV. Particularly, we have been interested in the response to protons incident at a non-normal angle on CR39, which presents challenges in characterizing the detection efficiency of CR39. Most CR39 discussions assume normal incidence, but the non-normal case is an important question to study for proposed neutron spectrometers that involve scattered protons reaching CR39 at oblique angles.

Our study of angles up to 50 degrees offered a number of insights into the behavior of CR39 with angled protons. We concluded that, in our energy regime (< 3 MeV), incident angles beyond 45 degrees produced no usable data. In general, the angles above 30 degrees were shown to be impractical for spectrometer design; detection efficiency at 30 degrees is noticeably lower than that at 0 degrees in all cases.

Up through 25 degrees, we have a usable energy range between 1.0 and 2.1 MeV where detection efficiency is unaffected. Moreover, at a small angled offset of 10 degrees this region of full detection efficiency extends through 2.9 MeV. We can hypothesize that neutron spectrometers involving these energy and angle parameters will be reliable in ICF applications. We extrapolate from our 2.4 and 2.9 MeV data that the "critical angle" at which detection efficiency drops noticeably will decrease as proton energy increases above 2.9 MeV. Experimental trials with different fusion reactions producing higher energy protons could be used to test this hypothesis.

The data is inconclusive at low energies in the range ≤ 0.8 MeV. Here we reach the lower energy end of CR39's detection capability, as we notice the 4 and 5 hour etch data showing a detection efficiency drop off even at 0 degrees. However, the extent to which the incident angle plays a role is unclear given the change in energy associated with angled filters. A specific study of low energy incidence on CR39 with finer energy increments could help resolve these details.

Finally, the experimental data allows for comparisons with similar results made through simulations. Our results showed much more limited detection ranges than theoretical models predicted. These models simulated the related case of neutrons scattering protons within CR39. We concluded that incident protons have a much more limited range of angles and energies to

achieve 100% CR39 detection than those in the model. These limitations shown through experiment should be considered when designing neutron spectrometers for laser facilities.

6. References

[1] S. Atzeni and J. Meyer-ter-Vehn, The Physics of Inertial Fusion, Oxford Univeristy Press, 2009.

[2] M. Kikuchi, K. Lackner and M. Q. Tran, Fusion Physics, Vienna: International Atomic Energy Agency, 2012.

[3] T. R. Boehly et al., *Optical Communications,* vol. 133, no. 495, 1997.

[4] M. Cuneo, M. C. Herrmann, D. B. Sinars, S. A. Slutz, W. A. Stygar, R. A. Vesey, A. B. Sefkow, G. A. Rochau, G. A. Chandler, J. E. Bailey, J. L. Porter, R. D. McBride, D. C. Rovang, M. G. Mazarakis, E. P. Yu, D. C. Lamppa and K. J. Peterson, *IEEE Transactions on Plasma Science,* vol. 40, 2012.

[5] G. H. Miller, E. I. Moses and C. R. Wuest, *Nuclear Fusion,* vol. 44, 2004.

[6] S. A. Durrani and R. K. Bull, Solid State Nuclear Track Detections, Principles, Methods and Applications, New York: Pergamon, 1987.

[7] F. H. Seguin, J. A. Frenje, C. K. Li, D. G. Hicks, S. Kurebayashi, J. R. Rygg, B. E. Schwartz, R. D. Petrasso, S. Roberts, J. M. Soures, D. D. Meyerhofer, T. C. Sangster, J. P. Knauer, C. Sorce, V. Yu, C. Stoeckl, T. W. Phillips, R. J. Leeper, K. Fletcher and S. Padalino, "Spectrometry of charged particles from inertial-confinement-fusion plasmas," *Review of Scientific Instruments,* vol. 74, no. 2, 2003.

[8] N. Sinenian, M. J. E. Manuel, A. B. Zylstra, M. Rosenberg, H. G. Rinderknecht, D. T. Casey, M. Gatu Johnson, J. A. Frenje, F. H. Seguin, C. K. Li, R. D. Petrasso and S. C. McDuffee, "The response of CR-39 nuclear track detector to 1-9 MeV protons," *Review of Scientific Instruments,* vol. 82, 2011.

[9] B. Lahmann, M. Gatu Johnson, K. D. Hahn, J. A. Frenje, D. J. Ampleford, B. Jones, M. A. Mangan, A. Maurer, C. L. Ruiz, F. H. Seguin and R. D. Petrasso, "A Neutron Recoil-Spectrometer for Measuring Yield and Determining Liner Areal Densities at the Z Facility," *To be submitted to RSI.*

[10] N. Sinenian, M. J. E. Manuel, A. B. Zylstra, M. Rosenberg, C. J. Waugh, H. G. Rinderknecht, D. T. Casey, H. Sio, J. K. Ruszczynski, L. Zhou, M. Gatu Johnson, J. A. Frenje, F. H. Seguin, C. K. Li, R. D. Petrasso, C. L. Ruiz and R. J. Leeper, "Upgrade of the MIT Linear Electrostatic Ion Accelerator (LEIA) for nuclear diagnostics development for Omega, Z and the NIF," *Review of Scientific Instruments,* vol. 83, 2012.

[11] J. F. Ziegler, M. D. Ziegler and J. P. Biersack, "SRIM - The stopping and range of ions in matter," *Nuclear Instruments and Methods in Physics Research,* vol. 268, no. 11-12, 2010.

[12] MIT Plasma Science and Fusion Center, "LEIA Wiki," 2020. [Online]. Available: https://leia.psfc.mit.edu/wiki/index.php/Main_Page.

[13] N. Sinenian, M. Manuel, M. Rosenberg and J. Frenje, "Standard Operating Procedure for the accelerator maintained by the HEDP division," 2009. [Online]. Available: https://leia.psfc.mit.edu/files/sop/Accelerator%20SOP%202009-10-01%20-%20MM-MR.pdf.

[14] J. A. Frenje, C. K. Li, F. H. Seguin, D. G. Hicks, S. Kurebayashi, R. D. Petrasso, S. Roberts, V. Yu, D. Glebov, D. Meyerhofer, T. C. Sangster, J. M. Soures, C. Stoeckl, C. Chiritescu, G. J. Schmid and R. A. Lerche, "Absolute measurements of neutron yields from DD and DT implosions at the OMEGA laser facility using CR-39 track detectors," *Review of Scientific Instruments,* vol. 73, no. 7, 2002.